THE JOURNAL OF PHYSICAL CHEMISTRY C

ARTICLE

pubs.acs.org/JPCC

Silver Nanoparticles Enhanced Upconversion Luminescence in Er^{3+}/Yb^{3+} Codoped Bismuth-Germanate Glasses

Yi Wu,[†] Xiang Shen,[†] Shixun Dai,[*,†] Yinsheng Xu,[‡] Feifei Chen,[†] Changgui Lin,[‡] Tiefeng Xu,[*,†] and Qiuhua Nie[†]

[†]Faculty of Information Science and Engineering, Ningbo University, Ningbo, 315211, China

[‡]Faculty of Materials Science and Chemical Engineering, Ningbo University, Ningbo, 315211, China

Supporting Information

ABSTRACT: Surface plasmon resonance (SPR) of noble metal nanoparticles (NPs) fostered a new area of nanophotonics, especially in the selective photon absorption and scattering. The precipitation of Ag NPs in glass would enhance the emission efficiency. Here, we studied the effects of annealing temperature (resulted in the increased Ag NPs' concentration) or AgCl concentration on the luminescence properties of Er^{3+}/Yb^{3+} codoped bismuth-germanate glasses which were synthesized by a single-step melting−quenching technique. The SPR peak of Ag NPs appears around 600 nm, and the size of precipitated Ag NPs (spherical, hexagonal) ranges from 5 to 15 nm. With the precipitation of the Ag NPs, more intense green (527 nm, 548 nm) and red (661 nm) upconversion (UC) emission bands are observed up to 7.7, 10.1, and 6.5 folds in the glass containing 1 wt % AgCl annealed at 480 °C for 24 h, respectively. The Ag NPs embedded glasses showed significantly local field change that allowed for more bright UC emission by SPR.

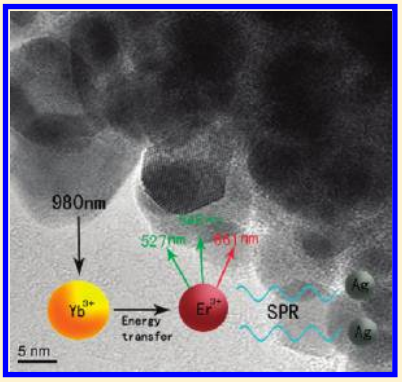

1. INTRODUCTION

In the past decades, upconversion (UC) luminescence of rare-earth (RE) ions has attracted much interest in their capability of converting infrared radiation into visible light.[1−5] However, the converting efficiency is relatively low ($\eta = 10^{-3}$)[6] due to the very small absorption coefficients of most lanthanide ions.[7,8] To overcome this drawback, sensitizer ions (such as Yb^{3+}) or nanocrystals embedded in the host glass were investigated.[9−12] Recently, surface plasmon resonance (SPR) of noble metal nanoparticles (NPs) gives another choice to enhance the emission efficiency. The SPR of gold and silver NPs is a remarkable phenomenon that already has fostered many new powerful analytical techniques and applications.[13−16] Generally, gold and silver particles with diameters larger than 5 nm show strong plasmon absorption and therefore enhance the luminescence by a plasmonic near-field enhancement in a typical distance between 1 and 10 nm.[16] In such situation, the lanthanides' photonic mode density would be enhanced tremendously by the interaction between metal particles and lanthanide. And then boost excitation efficiency as well as the radiative decay rate. In other words, when the wavelength of the incident light beam or the luminescence wavelength approximately near the SPR wavelength of metallic NPs, the large luminescence enhancement can be obtained.[17,18] The enhancement of the RE luminescence has been realized in the glasses with the silver NPs. da Silva et al. found a significant enhancement of the UC luminescence in the PbO-GeO_2 glasses containing silver NPs.[19] The influence of silver NPs on the luminescence of Pr^{3+} doped TeO_2−PbO-GeO_2 was investigated in ref 20. Also the large influence of gold NPs in the UC luminescence of Eu^{3+}-doped GeO_2−Bi_2O_3 was reported.[21]

As mentioned above, both the sensitizer and the metal NPs can enhance the luminescence. By introducing both of them, the more intense emission may be realized. In fact, an enhancement of the UC emission has been found in Tm^{3+}/Yb^{3+} codoped PbO-GeO_2 glass containing silver NPs.[22] However, no more research has been reported on this subject.

In this paper, we observed a significant enhancement of the UC emission of Er^{3+}/Yb^{3+} ions in the bismuth-germanate (BGN) glasses containing Ag NPs. The Er^{3+}/Yb^{3+} codoped BGN glasses containing Ag were synthesized by a melting−quenching technique. To simplify the precipitation of Ag NPs, a single-step method was utilized. The quenched glasses were annealed at different temperature for the same duration and the Ag NPs obtained without the further heat treatment. The effect of annealing temperature or AgCl concentration on the emission properties have been investigated, and the luminescence mechanism has been proposed.

2. EXPERIMENTAL SECTION

The glass samples with the nominal composition 53.3$BiO_{1.5}$-33.3GeO_2-13.4$NaO_{0.5}$ (BGN, in mol %) were synthesized by a single-step melting−quenching technique. As shown in Table 1,

Received: July 23, 2011
Revised: November 14, 2011
Published: November 15, 2011

Table 1. Dopants Concentration and Annealing Conditions of Glass $53.3BiO_{1.5}$-$33.3GeO_2$-$13.4NaO_{0.5}$

		dopants (wt %)			annealing	
series	sample	Er_2O_3	Yb_2O_3	AgCl	temperature (°C)	duration (h)
A	Ag0-G390	0.3	3	0	390	24
	Ag1-G390			1	390	
	Ag1-G420			1	420	
	Ag1-G450			1	450	
	Ag1-G480			1	480	
	Ag1-G510			1	510	
B	Ag0-G480	0.3	3	0	480	24
	Ag0.5-G480			0.5		
	Ag1-G480			1		
	Ag2-G480			2		
C	BGN	0	0	0	480	24
	Ag1-G			1		

different concentrations of Er_2O_3, Yb_2O_3, and AgCl were introduced as luminescent center, sensitizer, and metal (Ag) NPs, respectively. Reagents (10 g) were melted in a corundum crucible at 1200 °C for 30 min and quenched in air in a preheated brass mold. To precipitate the Ag and eliminate the inner stress, the glasses were then annealed at 390, 420, 450, 480, and 510 °C for 24 h and cooled to room temperature, respectively. The glass transition temperature of the host is 450 °C, which was determined by Q2000 differential scanning calorimetry (TA Instruments, USA). These samples were labeled as Ag1-G390, Ag1-G420, Ag1-G450, Ag1-G480, and Ag1-G510, respectively. For comparison, the BGN glass without silver NPs was also prepared and annealed at 390 °C (Ag0-G390). The glasses with different Ag concentrations (x = 0, 0.5, 1, 2 wt %) were synthesized in a similar technique annealed at 480 °C for 24 h. These samples were labeled as Ag0-G480, Ag0.5-G480, Ag1-G480, and Ag2-G480, respectively. The base glass (BGN) and only Ag-doped glass (Ag1-G) were also prepared and annealed at 480 °C for 24 h as references. Finally, the samples were cut and well polished to meet the requirements for optical measurements.

X-ray diffraction (XRD) data were collected using a Bruker AXS D8 Advance diffractometer (Voltage 50 kV, current 40 mA, Cu Ka) with a step width of 0.02°. Scanning electron microscopy (SEM) was carried out by coating the glass samples with platinum in an argon atmosphere using Tescan VEGA 3SBH SEM. To investigate the nucleation of silver NPs, a 200 kV transmission electron microscope (TEM, Model: Tecnai F20) was used. Refractive index (RI, λ = 1550 nm) of the host BGN glass was measured by prism minimum deviation method (SPA-4000). Absorption spectra were measured with a Lamda 950UV/VIS/NIR spectrophotometer in the range of 300−3000 nm. Luminescence spectra were collected with a TRIAX550 spectrofluorimeter upon excitation of a 980 nm laser diode. The absorbed photon numbers were determined by collecting the emission spectra under different pumping laser power. All measurements were performed at room temperature.

3. RESULTS AND DISCUSSION

To be sure the Ag precipitated purely, the annealing temperature is carefully controlled lower than the T_g (450 °C). However, there is no other crystallization until the temperature up to 480 °C.

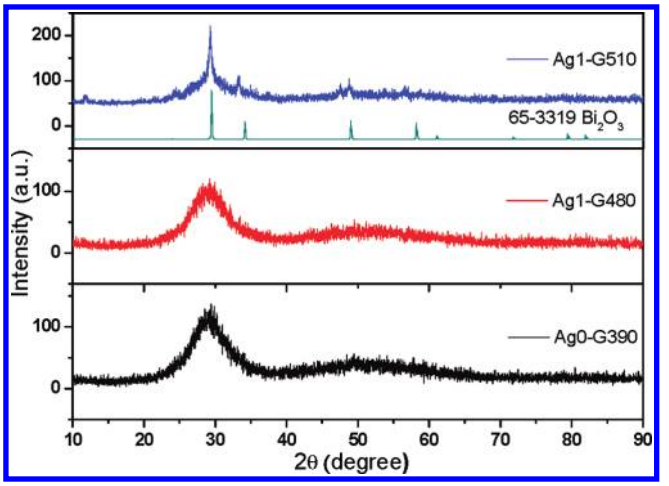

Figure 1. XRD patterns of samples Ag0-G390, Ag1-G480, and Ag1-G510, respectively.

As Figure 1 shows, only the glass annealed at 510 °C shows several acute peaks, indicating no glass crystallization can be seen under 480 °C. Diffraction peaks of the glass annealed at 510 °C are mainly attributed to Bi_2O_3 phases, the color of the glasses, and the SEM images in Figure 2 support the above analysis. As shown in Figure 2, only the glass sample which was annealed at 510 °C become devitrification and the SEM images also show the same result.

To verify the precipitation of Ag NPs, TEM was conducted on sample Ag0-G390 and Ag1-G420. Parts a and b of Figure 3 show TEM images of the sample without silver NPs (Ag0-G390) and the sample containing silver NPs annealed at 420 °C for 24 h (Ag1-G420). Clearly, small spherical and hexagonal NPs can be seen in Figure 3b. As shown in Figure 3b Ag NPs are closely dispersed and partial NPs aggregate in the glass, and the size ranges from 5 to 15 nm. To further confirm the Ag state, selected area electron diffraction pattern (SAED) was also performed on samples Ag0-G390 and Ag1-G420. No diffraction pattern was shown in Figure 3c for sample Ag0-G390, whereas diffraction patterns characteristic of silver crystals were identified in Figure 3d for sample Ag1-G420. The SAED image (Figure 3d) depicts the presence of (111) crystallographic planes of Ag NPs. A probable mechanism of Ag NPs precipitation has been explained by considering the reduction potentials (E^0) of the thermochemical reaction. As we all know, raw material Bi_2O_3 will be easily reduced to its lower valence state when melted at a higher temperature (1200 °C).[23,24] By comparison of the standard reduction potential (Table S1 of Supporting Information) of various species,[25,26] it is clear that the standard potential of Ag^+/Ag^0 is much higher (0.80 V) than that of Bi^{3+}/Bi^0 (0.31 V). By use of the standard reduction potential, the calculated Gibbs free energy ($\Delta G^0 = -nFE^0$) of Bi^{3+}/Bi^0 is −89 KJ and Ag^+/Ag^0 is −77 KJ. Thus the Ag^+ would reduce first than that of Bi^{3+}. Similar observation has also been reported by Singh et al. in the potassium bismuth borate glass matrix.[27]

After annealed at different temperatures for 24 h, the absorption spectra of Er^{3+}/Yb^{3+} codoped glass without silver NPs and glasses containing 1 wt % silver NPs have two remarkable changes as Figure 4a shows. The first is the obvious blue shift of bandgap wavelength with the addition of AgCl, which may come from the following two aspects: (i) The bandgap of the hosts is 2.75 eV,

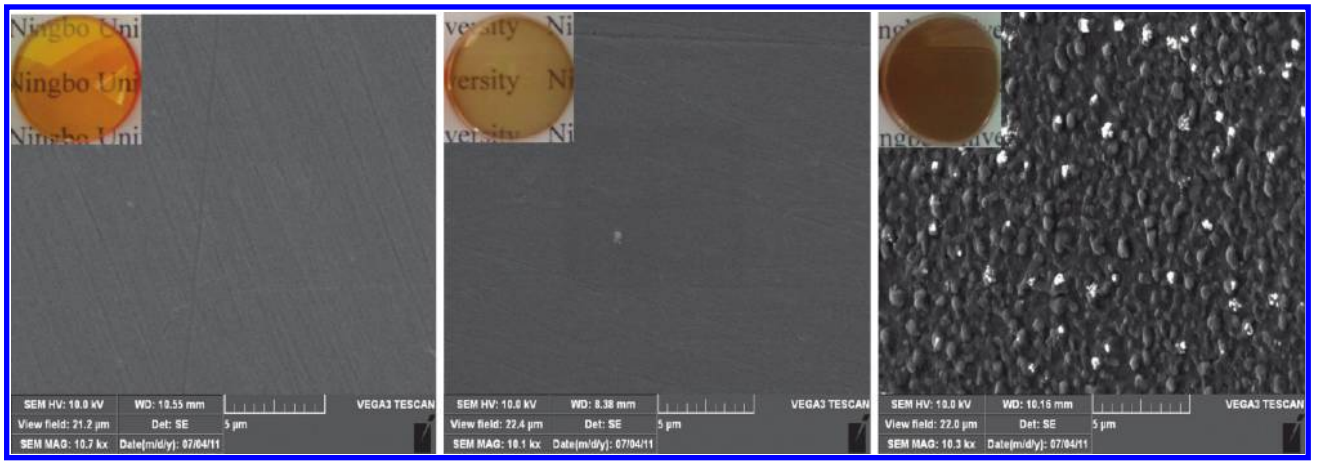

Figure 2. SEM images of samples Ag0-G390 (left), Ag1-G480 (middle), and Ag1-G510 (right), respectively. The insets are corresponding pictures of glass samples.

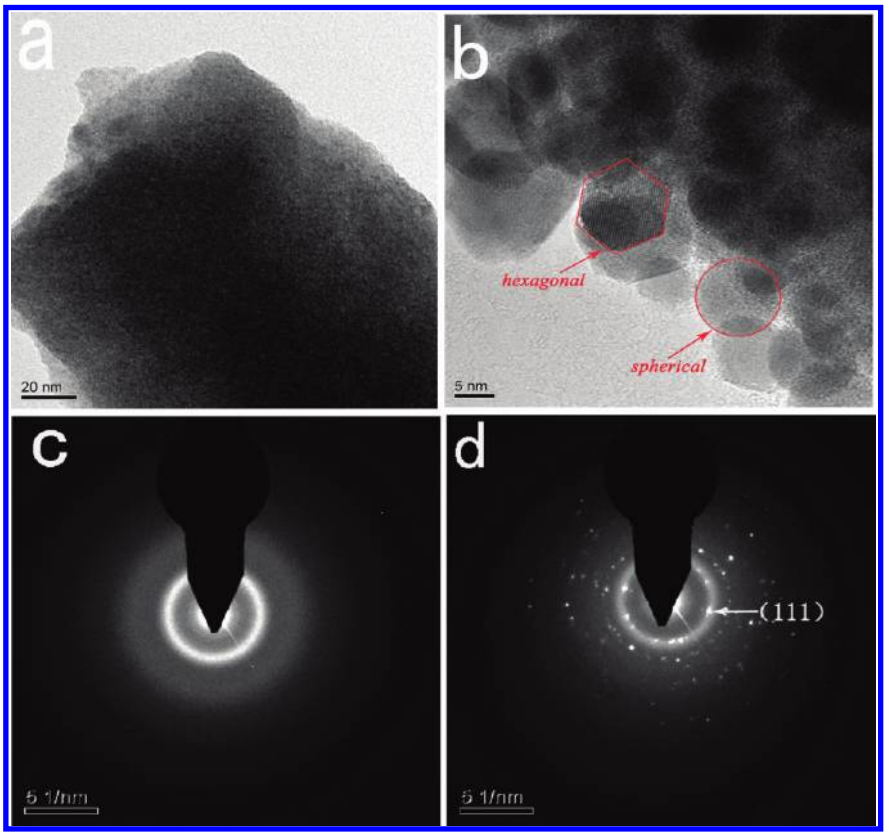

Figure 3. TEM images of Ag0-G390 (a) and Ag1-G420 (b). SAED of Ag0-G390 (c) and Ag1-G420 (d).

while both the bandgap of AgCl (3.25 eV) and Ag (4.0 eV) are larger than the hosts, so the addition of AgCl resulted in the blue shift of bandgap of the hosts.[28,29] (ii) The quantum size effect of Ag NPs in the glasses makes the bandgap wider, the energy of absorption transition higher, leading to the blue shift of bandgap of the hosts.[30,31] We can also observe the typical SPR band of Ag^0 NPs on the absorption spectra is around 600 nm and becomes more intense with increasing annealing temperature. The absorption for the glass absence of Er^{3+}/Yb^{3+} confirmed the Ag SPR band and the blue shift of the bandgap (Figure S1 of Supporting Information). The plasmon peak position was mainly influenced by the refractive index (RI) of glass matrix.[32] It is well know that the classic location of Ag SPR peak of silicate glasses (RI =1.45−1.5) lies in the 410 nm region.[33,34] For the present glass which has the RI around 2.02, the Ag SPR peak would be shifted toward longer wavelength compared to that of silicate glasses. In fact, the Ag SPR band appeared around 600 nm and increased with increasing annealing temperature due to the population of the Ag NPs. A similar phenomenon has also been observed in the absorption spectra of Er^{3+}/Yb^{3+} codoped glass without silver NPs and glasses containing different concentrations of silver NPs annealed at 480 °C as Figure 4b shown.

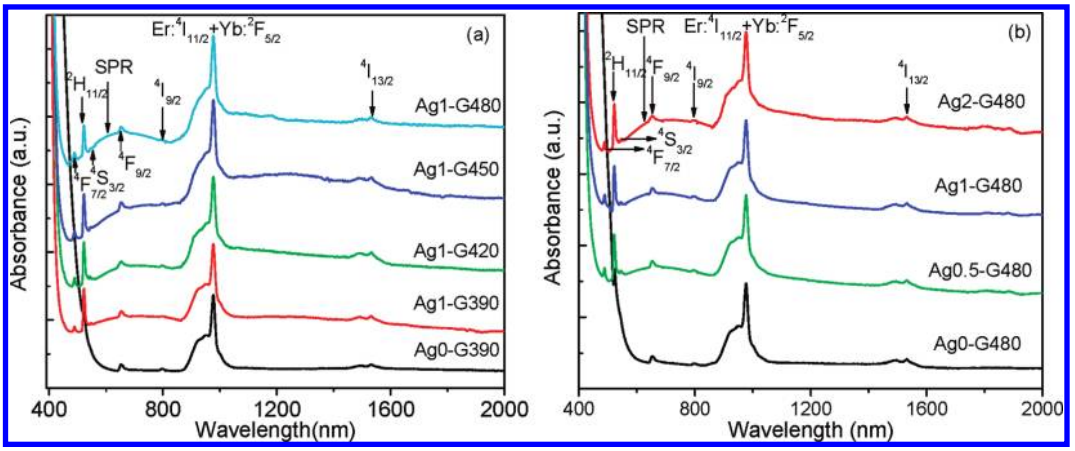

Figure 4. Absorption spectra of Er^{3+}/Yb^{3+} codoped glass and glasses (a) containing 1 wt % Ag NPs annealed for different temperature; (b) containing different concentrations of Ag NPs annealed at 480 °C.

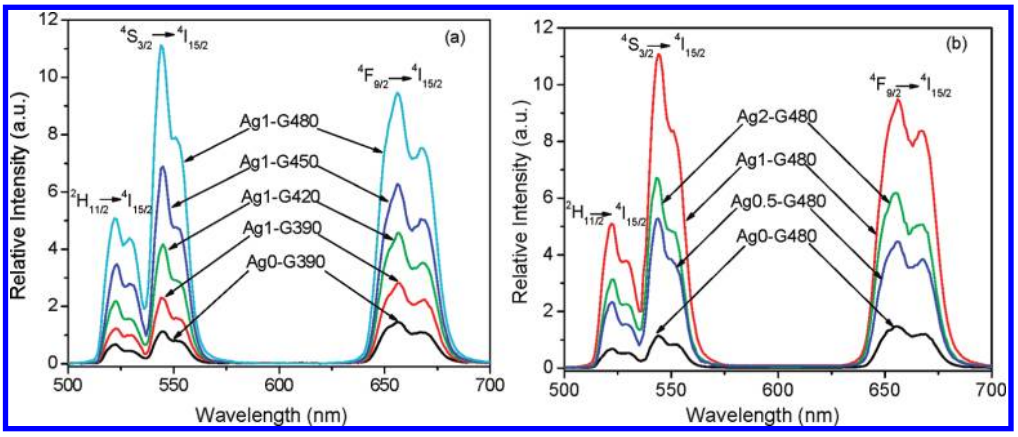

Figure 5. UC emission spectra of Ag and Er^{3+}/Yb^{3+} codoped BGN glasses (a) containing 1 wt % Ag NPs annealed for different temperature and (b) containing different concentrations of Ag NPs annealed at 480 °C. The spectrum for the sample without Ag NPs is also shown to illustrate the luminescence enhancement.

Parts a and b of Figure 4 also show the features associated to the Er^{3+}:4f−4f transitions originated from the ground state $^4I_{15/2}$. The strong absorption band around 980 nm is mainly due to the Yb^{3+}:$^2F_{7/2}\rightarrow{}^2F_{5/2}$ transition that overlaps with the weaker Er^{3+}:$^4I_{15/2}\rightarrow{}^4I_{11/2}$ transition of the ions.

After the precipitation of the Ag NPs, the SPR would enhance the emission around 600 nm. Figure 5a shows the UC emission spectra of Er^{3+}/Yb^{3+} codoped BGN samples annealing at different temperature. Under the 980-nm excitation, the strong green emissions (527 and 548 nm) along with the red emission (661 nm) were observed at room temperature. The UC emission spectra of glass absence Er^{3+}/Yb^{3+} confirmed Ag NPs did not emit any photon under 980 nm excitation (Figure S2 of Supporting Information). These three emissions were from the $^2H_{11/2}\rightarrow{}^4I_{15/2}$, $^4S_{3/2}\rightarrow{}^4I_{15/2}$, and $^4F_{9/2}\rightarrow{}^4I_{15/2}$ transitions, respectively. The UC luminescence intensity of the samples increased rapidly with the increasing annealing temperature, exhibiting the maximum value at 480 °C. Interestingly, the relative integrated intensity of the emission bands centered at 527, 548, and 661 nm have been increased up to 7.7, 10.1, and 6.5 folds for sample Ag1-G480 with respect to the host Ag0-G390 glass, respectively. It is well-known that $^2H_{11/2}\rightarrow{}^4I_{15/2}$, $^4S_{3/2}\rightarrow{}^4I_{15/2}$, and $^4F_{9/2}\rightarrow{}^4I_{15/2}$ transitions of Er^{3+} ions are electric dipole transitions, which are very sensitive to the local field.[35] The present Ag^0 NPs in the glass host enhance the local field around Er^{3+} ions and show a strong plasmon absorption band covering the above-mentioned three transitions. Therefore, the $^2H_{11/2}\rightarrow{}^4I_{15/2}$ (527 nm), $^4S_{3/2}\rightarrow{}^4I_{15/2}$ (548 nm), and $^4F_{9/2}\rightarrow{}^4I_{15/2}$(661 nm) UC emissions have been enhanced. Interestingly, the higher annealing temperature, the more intense SPR band. So the UC emission intensity of the above three transitions are also increased as the increasing annealing temperature. Besides, we observe that the transition Er^{3+}:$^4S_{3/2}\rightarrow{}^4I_{15/2}$ (548 nm) is more sensitive to the presence of silver NPs than the transitions Er^{3+}:$^2H_{11/2}\rightarrow{}^4I_{15/2}$ (527 nm) and $^4F_{9/2}\rightarrow{}^4I_{15/2}$ (661 nm), while fluorescence bands at 527 and 661 nm have the similar enhancement. Our previous work[36] has shown that the populations of $^2H_{11/2}$ and $^4S_{3/2}$ energy levels are strongly affected by the temperature (T) and their energy separation (ΔE). It can be expressed as follows

$$R = C\exp\left(-\frac{\Delta E}{KT}\right) \quad (1)$$

where R is the integrated emission intensity ratio between $^2H_{11/2}\rightarrow{}^4I_{15/2}$ and $^4S_{3/2}\rightarrow{}^4I_{15/2}$ transitions and also proportional to populations distribution of above two levels. C is a parameter

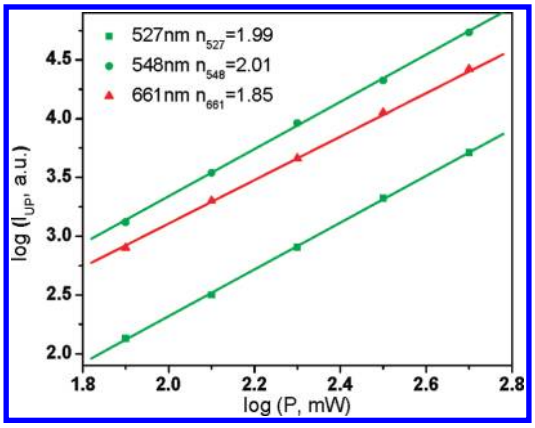

Figure 6. Log−log plots of UC fluorescence emissions for glass Ag1-G480 as a function of the 980 nm pump power.

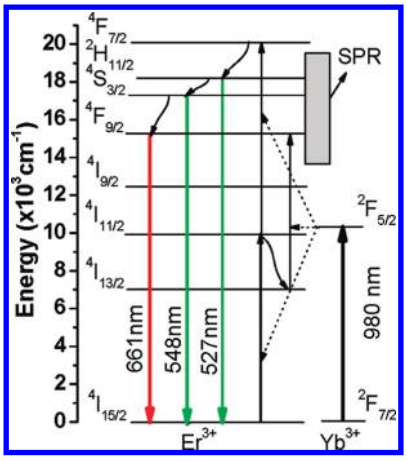

Figure 7. Simplified energy level of Er^{3+} and Yb^{3+} ions and possible UC pathways for the Er^{3+}/Yb^{3+} codoped BGN glasses.

related to the degeneracy and spontaneous emission rates of the $^2H_{11/2}$ and $^4S_{3/2}$ levels. K is the Boltzmann's constant. From this equation, local field around Er^{3+} ions enhancement induced by Ag^0 SPR will lead to the change of the energy gap ΔE, which makes the populations on the $^2H_{11/2}$ and $^4S_{3/2}$ levels redistribute. This may be why the $^2H_{11/2} \rightarrow {}^4I_{15/2}$ (527 nm) and $^4F_{9/2} \rightarrow {}^4I_{15/2}$ (548 nm) transitions have different enhancement folds. In addition, the plasmon absorption band responds asymmetrically to the enhancement of mentioned three UC emissions because of their energy mismatch with resonance center of Ag^0 NPs. Similar results were also obtained in the UC emission spectra of Er^{3+}/Yb^{3+} codoped BGN samples containing different concentrations of Ag NPs annealing at 480 °C (Figure 5b). The maximum luminescence enhancement has been found to occur at Ag concentration of 1 wt %. The luminescence enhancement is also resulted from local field enhancement effect induced by Ag^0 NPs. The decrease in intensity of all the fluorescence peaks at higher Ag concentration (2 wt %) is due to plasmon reabsorption as a consequence of increased quantity of Ag NPs aggregates.[37]

It is known that the UC emission intensity I_{UP} depends on the laser intensity P according to the relation $I_{UP} \propto P^n$, where n is the number of photons participating in the UC process.[38,39] The plot of log I_{UP} vs log P yields a straight line with slope n. For the 527, 548, and 661 nm emissions, n is 1.99, 2.01, and 1.85, respectively, indicating that the processes for the three emissions are based in successive two photon absorptions, as shown in Figure 6.

According to the energy matching and quadratic dependence on excitation power, the possible UC mechanisms for the emissions are presented based on the energy level diagram of Er^{3+} and Yb^{3+} in Figure 7. Under 980 nm pumping, the Yb^{3+} ions are first excited from the ground state $^2F_{7/2}$ to the excitation state $^2F_{5/2}$. Then, the excited Yb^{3+} ions transfer the energy to the Er^{3+} ions that are excited from the $^4I_{15/2}$ ground state to the $^4I_{11/2}$ state. Afterward, a second electron transfer event promotes the Er^{3+} ions from the $^4I_{11/2}$ level to the $^4F_{7/2}$ level. The populated Er^{3+}:-$^4F_{7/2}$ level then relaxes rapidly and nonradiatively to the next lower levels $^2H_{11/2}$ and $^4S_{3/2}$ resulting from the small energy gap between them. The $^2H_{11/2}$ level is populated from the $^4S_{3/2}$ via thermal equilibrium between them, which is very small at the experimental temperature. Consequently the band at 527 nm due to $^2H_{11/2} \rightarrow {}^4I_{15/2}$ transition has a weak intensity.[40] The above processes then produce the two green emissions centered at 527 and 548 nm, respectively. The red emission at 661 nm is originated from the $^4F_{9/2} \rightarrow {}^4I_{15/2}$ transition. There exist two main possible pumping mechanisms for the red emission in the BGN glass. The first is the feeding of the $^4F_{9/2}$ level through the nonradiative relaxation from the $^4S_{3/2}$ level. In the other possible mechanism, the population of $^4F_{9/2}$ is based on the processes as follows: electron transfer from Yb^{3+}, $^2F_{5/2}$ (Yb^{3+}) + $^4I_{13/2}$ (Er^{3+}) → $^2F_{7/2}$(Yb^{3+}) + $^4F_{9/2}$(Er^{3+}); cross relaxation between Er^{3+} ions, $^4I_{13/2} + {}^4I_{11/2} \rightarrow {}^4I_{15/2} + {}^4F_{9/2}$; excited-state absorption, $^4I_{13/2}$ + a photon → $^4F_{9/2}$. The $^4I_{13/2}$ level is populated owing to the nonradiative relaxation from the upper $^4I_{11/2}$ level.

4. CONCLUSION

The Er^{3+}/Yb^{3+} codoped bismuth-germanate glasses containing silver NPs (spherical, hexagonal) have been synthesized by a single-step melting−quenching technique. The absorption spectra show the SPR peak of Ag NPs appears around 600 nm. It was demonstrated that the silver NPs play an important role in the Er^{3+} luminescence enhancement. With the precipitation of the Ag NPs, more intense green (527, 548 nm) and red (661 nm) UC emission bands were observed up to 7.7, 10.1, and 6.5 folds in the glasses annealed at 480 °C for 24 h, respectively. The enhanced UC emission in the visible region is attributed to the increased local field around the Er^{3+} ions and the plasmon absorption band responds asymmetrically to the enhancement of mentioned three UC emissions because of their energy mismatch with resonance center of Ag^0 NPs. A two-photon process is involved in this UC emission. The single-step melting−quenching technique provides a simplified way to synthesize the high-efficiency UC luminescent materials.

■ ASSOCIATED CONTENT

Supporting Information. Standard reduction potential (Table S1) and the absorption and UC emission spectra of the host and 1 wt % Ag doped BGN glass (Figures S1 and S2). This information is available free of charge via the Internet at http://pubs.acs.org.

■ AUTHOR INFORMATION

Corresponding Author

*E-mail: daishixun@nbu.edu.cn (S.D.); xutiefeng@nbu.edu.cn (T. X.).

■ ACKNOWLEDGMENT

Supported by Program for New Century Excellent Talents in University (No. NCET-09-1076), Zhejiang Provincial Natural Science Foundation of China under Grant No. R1101263, Students Science and Technology Innovation Program of Zhejiang Province (No. 2010R405065), the Scientific Research Foundation of Graduate School of Ningbo University (No. G10JA004), Student Research and Innovation Program of Ningbo University, and K. C. Wong Magna Fund in Ningbo University.

■ REFERENCES

(1) Aisaka, T.; Fujii, M.; Hayashi, S. *Appl. Phys. Lett.* **2008**, *92*, 132105–3.
(2) Yi, G. S.; Zhao, S. Y.; Ge, Y.; Yang, W. J.; Chen, D. P.; Guo, L. H. *Nano Lett.* **2004**, *4*, 2191–2196.
(3) Wang, L. Y.; Yan, R. X.; Li, Y. D. *Angew. Chem., Int. Ed.* **2005**, *44*, 6054–6057.
(4) Sanders, S.; Waarts, R. G.; Mehuys, D. G.; Wetch, D. F. *Appl. Phys. Lett.* **1995**, *67*, 1815–1817.
(5) Jacinto, C.; Vermelho, M. V. D.; Gouveia, E. A; de Araujo, M. T; Udo, P. T; Astrath, N. G. C; Baesso, M. L *Appl. Phys. Lett.* **2007**, *91*, 071102–3.
(6) Auzel, F. *Chem. Rev.* **2004**, *104*, 139–174.
(7) Singh, S. K.; Giri, N. K.; Rai, D. K.; Rai, S. B. *Solid State Sci.* **2010**, *12*, 1480–1483.
(8) Som, T.; Karmakar, B. *J. Opt. Soc. Am. B* **2009**, *26*, B21–B27.
(9) Boyer, J. C.; Vetrone, F.; Capobianco, J. A.; Speghini, A.; Bettinelli, M. *Chem. Phy. Lett.* **2004**, *390*, 403–407.
(10) Diening, A.; Kück, S. *J. Appl. Phys.* **2000**, *87*, 4063–4068.
(11) Kassab, L. R. P.; Fukumoto, M. E.; Gomes, L. *J. Opt. Soc. Am. B* **2005**, *22*, 1255–1259.
(12) Zheng, C. B.; Xia, Y. Q.; Qin, F.; Yua, Y.; Miao, J. P.; Zhang, Z. G.; Cao, W. W. *Chem. Phys. Lett.* **2010**, *496*, 316–320.
(13) Kim, S.; Jin, J.; Kim, Y. J.; Park, I. Y.; Kim, Y.; Kim, S. W. *Nature* **2008**, *453*, 757–760.
(14) Mertens, H.; Polman, A. *Appl. Phys. Lett.* **2006**, *89*, 211107–3.
(15) Le, F.; Brandl, D. W.; Urzhumov, Y. A.; Wang, H.; Kundu, J.; Halas, N. J.; Aizpurua, J.; Nordlander, P. *ACS Nano* **2008**, *2*, 707–718.
(16) Eichelbaum, M.; Rademann, K. *Adv. Funct. Mater.* **2009**, *19*, 2045–2052.
(17) Geddes, C. D.; Lakowicz, J. R. *J. Fluor.* **2002**, *12*, 121–129.
(18) Lakowicz, J. R. *Anal. Biochem.* **2001**, *298*, 1–24.
(19) da Silva, D. M.; Kassab, L. R. P.; Lüthi, S. R.; de Araújo, C. B.; Gomes, A. S. L.; Bell, M. J. V. *Appl. Phys. Lett.* **2007**, *90*, 081913–3.
(20) Kassab, L. R. P.; de Araújo, C. B.; Kobayashi, R. A.; Pinto, R. A.; Da Silva, D. M. *J. Appl. Phys.* **2007**, *102*, 103515–4.
(21) Kassab, L. R. P.; Da Silva, D. M.; Pinto, R. A.; de Araújo, C. B. *Appl. Phys. Lett.* **2009**, *94*, 101912–3.
(22) Assumpção, T. A. A.; da Silva, D. M.; Kassab, L. R. P.; de Araújo, C. B. *J. Appl. Phys.* **2009**, *106*, 063522–4.
(23) Singh, S. P.; Karmakar, B. *Opt. Mater.* **2011**, *33*, 1760–1765.
(24) Zhang, Y.; Yang, Y.; Zheng, J.; Hua, W.; Chen, G. *J. Am. Ceram. Soc.* **2008**, *91*, 3410–3412.
(25) Vanýsek, P. Electrochemical series. In *CRC hand book of chemistry and physics*; Lide, D. R., Ed.; CRC: London, 1994.
(26) Lee, J. D. *Concise Inorganic Chemistry*, 5th ed; Backwell Science: London, 1996.
(27) Singh, S. P.; Karmakar, B. *Plasmonics* **2011**, *6*, 457–467.
(28) Fatti, N. Del.; Vallee, F. *Appl. Phys. B: Laser Opt.* **2001**, *73*, 383–390.
(29) Chen, F. F.; Dai, S. X.; Xu, T. F.; Shen, X.; Lin, C. G.; Nie, Q. H.; Liu, C.; Heo, J. *Chem. Phy. Lett.* **2011**, *514*, 79–82.
(30) Jiménez, J. A.; Liu, H.; Fachini, E. *Mater. Lett.* **2010**, *64*, 2046–2.
(31) Speranza, G.; Minati, L.; Chiasera, A.; Ferrari, M.; Righini, G. C.; Ischia, G. *J. Phys. Chem. C* **2009**, *113*, 4445–4450.
(32) Mulvaney, P. *Langmuir* **1996**, *12*, 788–800.
(33) Malta, O. L.; Santa-Cruz, P. A.; De Sá, G. F.; Auzel, F. *J. Lumin.* **1985**, *33*, 261–272.
(34) Som, T.; Karmakar, B. *J. Appl. Phys.* **2009**, *105*, 013102–8.
(35) Kalkman, J.; Kuipers, L.; Polman, A.; Gersen, H. *Appl. Phys. Lett.* **2005**, *86*, 041113–3.
(36) Shen, X.; Nie, Q. H.; Xu, T. F.; Dai, S. X.; Wang, X. S. *J. Lumin.* **2010**, *130*, 1353–1356.
(37) Nabika, H.; Deki, S. *J. Phys. Chem. B* **2003**, *107*, 9161–9164.
(38) Pollnau, M.; Gamelin, D. R.; Lüthi, S. R.; Güdel, H. U.; Hehlen, M. P. *Phys. Rev. B* **2000**, *61*, 3337–3346.
(39) Yeh, D. C.; Sibley, W. A.; Suscavage, M.; Drexhage, M. G. *J. Appl. Phys.* **1987**, *62*, 266–275.
(40) Som, T.; Karmakar, B. *Opt. Mater.* **2009**, *31*, 609–618.